Received: 26 January 2022 | Accepted: 5 April 2022

DOI: 10.1111/gcb.16230

Global Change Biology WILEY

RESEARCH ARTICLE

Explicit spatial modeling at the pore scale unravels the interplay of soil organic carbon storage and structure dynamics

Simon Zech[1] | Steffen A. Schweizer[2] | Franziska B. Bucka[2] | Nadja Ray[1] | Ingrid Kögel-Knabner[2,3] | Alexander Prechtel[1]

[1]Applied Mathematics (Modelling and Numerics), Department of Mathematics, Friedrich-Alexander-Universität Erlangen-Nürnberg (FAU), Erlangen, Germany

[2]Soil Science, Research Department Life Science Systems, TUM School of Life Sciences, Technical University of Munich, Freising-Weihenstephan, Germany

[3]Institute for Advanced Study, Technical University of Munich, Garching, Germany

Correspondence
Simon Zech, Applied Mathematics (Modelling and Numerics), Department of Mathematics, Friedrich-Alexander-Universität Erlangen-Nürnberg (FAU), Erlangen, Germany.
Email: simon.zech@fau.de

Funding information
Deutsche Forschungsgemeinschaft, Grant/Award Number: 251268514, 276972051 and 276973106

Abstract

The structure of soil aggregates plays an important role for the turnover of particulate organic matter (POM) and vice versa. Analytical approaches usually do not disentangle the continuous re-organization of soil aggregates, caught between disintegration and assemblage. This led to a lack of understanding of the mechanistic relationship between aggregation and organic matter dynamics in soils. In this study, we took advantage of a process-based mechanistic model that describes the interaction between the dynamic (re-)arrangement of soil aggregates, based on dynamic image analysis data of wet-sieved aggregates, to analyze the turnover of POM, and simultaneous soil surface interactions in a spatially and temporally explicit way. Our novel modeling approach enabled us to unravel the temporal development of aggregate sizes, organic carbon (OC) turnover of POM, and surface coverage as affected by soil texture, POM input, and POM decomposition rate comparing a low and high clay soil (18% and 33% clay content). Our results reveal the importance of the dynamic re-arrangement of soil structure on POM-related turnover of OC in soils. Firstly, aggregation was largely determined by the POM input fostering aggregates through additional gluing joints outweighing soil texture at lower decomposition rate, whereas at higher decomposition rate, soil texture had a higher influence leading to larger aggregates in the high clay soil. Secondly, the POM storage increased with clay content, showing that surface interactions may delay the turnover of OC into CO_2. Thirdly, we observed a structural priming effect in which the increased input of POM induced increased structural re-arrangement stimulating the mineralization of old POM. This work highlights that the dynamic re-arrangement of soil aggregates has important implications for OC turnover and is driven by underlying surface interactions where temporary gluing spots stabilize larger aggregates.

KEYWORDS
aggregates, clay content, OC turnover, POM degradation, soil structure dynamics, soil surface interactions, spatially explicit modeling, structural priming effect

1 | INTRODUCTION

Quantifying the fate of organic matter (OM) in soils is of high public relevance since soils harbor twice as much carbon as the atmosphere. Soil structure is directly related to OM dynamics as the break-up of soil aggregates and their formation influences the persistence of organic carbon (OC) in soils (Lehmann et al., 2020; Six et al., 2000; Virto et al., 2010). However, a neglect of soil structure

has been identified as an important omission in earth system or climate change modeling (Fatichi et al., 2020).

Organic matter enters soils mainly as particulate OM (POM), either through aboveground biomass or belowground biomass (Jastrow, 1996; Kögel-Knabner, 2002). Particulate organic matter is decomposed in soils, leading to a turnover into CO_2 and to a small extent also different organic compounds that interact with mineral particles and shape and enhance the soil structure (Kögel-Knabner, 2002; Totsche et al., 2018). The interactions between POM and the mineral matrix are highly relevant for the persistence of OM (Witzgall et al., 2021). Biogenically processed OM can modify the surface of soil particles, affecting the formation of aggregates (Guhra et al., 2022). The short-term turnover of OC induced by fresh input of OM was shown to be related to a range of microbial and root mechanisms (Jilling et al., 2021; Liang et al., 2018) whereas these processes have not been related so far with structural re-arrangement of soil aggregates. While many studies focused on the formation of aggregates and their interplay with OM dynamics, there is a lack of studies investigating the breakdown and destabilization of aggregates (Bailey et al., 2019). The experimental quantification of aggregation usually relies on their net formation or breakdown and methods to investigate the underlying counter-acting processes affecting the re-arrangement of soil structure are limited.

The clay content plays an important role in the formation of soil structure (Amézketa, 1999). Fine mineral particles have a relatively larger specific surface area (SSA), which implies more potential surface interaction with other particles and also OM. Consequently, high clay soils are usually connected with enhanced OC storage and aggregate formation (Schweizer et al., 2021; Souza et al., 2017; Stewart et al., 2008). The distribution of OM has been shown to be heterogeneous at the microscale (Keiluweit et al., 2012; Schweizer et al., 2018; Vogel et al., 2014; Wilhelm et al., 2022). Occluded POM particles have been postulated as nucleus for the formation of soil aggregates (Cotrufo et al., 2013; Golchin et al., 1994; Jastrow, 1996). Accordingly, different OM input was found to influence the size of soil aggregates (Bucka et al., 2021). Biogenic OM (microbial products, biofilms, dissolved OM) interacts with mineral surfaces, forming gluing agents (Chenu & Jaunet, 1992; Gaillard et al., 1999). Previous studies proposed that the formation of soil structure is mainly mediated by microbial processes rendering it as a "self-organized" system without external mechanical influence (Bucka et al., 2019; Crawford et al., 2012; Rabbi et al., 2020; Young & Crawford, 2004). While the effect of microbial processing was quantified by measuring the formed aggregates, the interactions with the arrangement and different types of organo–mineral surfaces warrants further analysis.

Modeling approaches can be used to shed light on the underlying processes. For a long time, these approaches have been limited to a macroscopic view using lumped parameters due to the lack of high resolution microscale information, the high heterogeneity and complexity of the processes, but also the lack of computational power (Bailey et al., 2018; Baveye et al., 2018; Pot et al., 2021). As Pot et al. (2021) have stated, the understanding of OM turnover processes should advance substantially with the help of new microscale modeling tools, which can be based on X-ray microtomography (μCT) images with resolutions down to a few microns. Such models allow assessing the dynamics of processes which cannot be observed experimentally, and to challenge hypotheses by varying the setting of simulation scenarios in silico. Pot et al. (2021) further elaborated the deficiencies of macroscopic models to describe the interaction of SOM turnover, microbial dynamics, and soil structure. They identified the need to account for physical protection of SOM to describe dynamic carbon turnover, to consider the spatially heterogeneous architecture of soils and to take into account organo–mineral interactions.

In this research, we address all these aspects and present a novel modeling approach that enables insights into the interplay of changing soil structure, the turnover of POM, and simultaneous modulation of soil surface properties that may enhance aggregations. We considered the structural re-organization of the soil architecture in a spatially and temporally explicit way. In contrast to most explicit microscale models based on static μCT images of intact soil cores as input data, our approach allowed us to incorporate the dynamic, self-organized re-arrangement of solid building units and POM and their surface interactions. For this we used a cellular automaton method (CAM) which extends a process-based mathematical model that was introduced by Ray et al. (2017) and Rupp et al. (2018). The CAM was successfully used to describe and study structure formation of microaggregates using minerals and oxides as idealized prototypic building units (Rupp et al., 2019; Zech et al., 2020). Zech, Ritschel, et al. (2022) further adapted and applied the model to study microbial population dynamics and the turnover of POM in microaggregates based on static μCT images. Here we integrated a dynamic re-arrangement of soil structure into CAM modeling.

For our dynamic model approach, we used experimental data of microaggregates and primary particles gained from dynamic image analyses of wet-sieved fractions of two agricultural topsoils with different clay contents (Schweizer et al., 2019). A crucial feature of the model is the distinction of reactive and non-reactive surface sites, as well as sites with a preference for POM-mineral bindings. In the presented scenarios, POM input was varied to study its effect on aggregation. To account for varying climate and environmental conditions (e.g. ambient temperatures), we considered different decomposition rates. The decomposition was dependent on the access to pore space, and thus allowed the development of occluded structures and the study of degradation beyond first-order rates. The age of the OC was monitored as well to study priming effects. We used the modeled scenarios to derive information about aggregate formation and turnover and development of POM, surface properties, and pore architecture. By this, we were able to elucidate the spatio-temporal organization during the complex process of soil structure formation. The mineralization of OM also allowed the quantification of the CO_2 production in the different scenarios. Thus, our model allowed to address the following research questions:

1. How do the factors soil texture, POM input, and POM decomposition rate impact soil aggregate formation and what is their relative importance?
2. How and to what extent does the addition of fresh POM shape the structural re-arrangement of soil aggregates and affect the decomposition of older POM into CO_2 for different textures?
3. How does the extent and type of surface coverage develop at different textures and possibly enhances aggregate structure formation and the turnover of POM?

2 | MATERIALS AND METHODS

2.1 | Conceptual model

Conceptually, soil aggregates consist of building units, namely primary particles, minerals, and POM particles (Totsche et al., 2018). Here, for the solid building units, we considered realistic image data of soil particle and aggregate shapes obtained by dynamic image analysis of wet-sieved aggregates, thus containing water-stable aggregates as well as primary particles (Section 2.2). The soil aggregates build a porous structure, while microporosity was disregarded in the following, and that changed dynamically with the pore space being filled by fluids (liquid or gas). Relocation of solid building units and POM particles can be caused or affected by, e.g. Brownian motion, OM compounds such as gluing agents, electric forces, and mechanical stresses due to, e.g., growing roots or earthworms. In this study, we focused on the role of surface effects and the impact of POM turnover on microaggregate formation. The reorganization of the porous structure was realized by a CAM as described in Section 2.3.

Part of the surface of the solid building units, depending on their size, was permanently marked as reactive (Chenu & Stotzky, 2002; Huang et al., 2015; McCarthy et al., 2008), with smaller building units having a higher proportion of reactive surface. At these reactive surfaces, POM particles may attach preferably undergoing microbial degradation (Witzgall et al., 2021). We considered the decomposition of POM particles to be influenced by the soil structure. The occlusion of POM within aggregates can constrain the accessibility for microbes. Consequently, the more occluded a POM particle is, the slower it is decomposed (Golchin et al., 1994; McCarthy et al., 2008). The microbial turnover of POM produces microbial remnants that may interact with the mineral particles serving as gluing agent for particle adhesion within the soil matrix (Hattori, 1988; Watteau et al., 2012). Such organo–mineral interfaces can temporarily cover mineral surfaces and probably enhance their surface reactivity as a gluing agent in the vicinity of the decomposing POM particle (Chenu & Stotzky, 2002; Huang et al., 2015; McCarthy et al., 2008). Temporary OM-covered mineral edges are assumed to provide gluing spots on mineral surfaces and enhance the formation of aggregates (Bucka et al., 2019). Based on the mineralization of OM, the gluing effect is temporarily limited. In accordance with adsorption studies (Gao et al., 2017, 2020), the surface conditioning effect of organic compounds on mineral surfaces (Dufrêne et al., 1999; Kleber et al., 2007) may be locally retained even after degradation of the OM coating. To account for the lasting increase of the mineral surface reactivity of such surface conditioning, we use the term "memory edges" for mineral surface edges after degradation of a neighboring OM cell. The precise specifications for the turnover of POM and OM-covered mineral edges are described in Section 2.4 and in detail in the Supporting Information.

Experiments have shown macroaggregate turnover between 40 and 60 days (De Gryze et al., 2005), macroaggregate formation after 1 month in incubation experiments (Bucka et al., 2019), and macroaggregate development within 3 months and decay after 12 months (Pronk et al., 2012). Since the total simulation time should be large enough to enable a representative turnover of aggregates, we set the total simulation time to 1000 days.

2.2 | Creating initial state of soil matrix models using dynamic image analyses

As the first step in the numerical model, we set up a dispersed initial distribution of solid building units and POM particles (Figures 1 and 2a). For this purpose, we created a particle shape library containing aggregates and primary particles of water-stable size fractions <250 μm imaged with a resolution of 2 μm from analyses of wet-sieved soil fractions (Schweizer et al., 2019). We considered these microaggregates <250 μm to remain stable during the modeled time frame of 1000 days as supported by radiocarbon dating of the contained OC (Pronk et al., 2013; Virto et al., 2010). To filter out odd-shaped particles, e.g. root pieces, or overlapping particles, we applied thresholds regarding the optical density of the images and sphericity of objects (Felde et al., 2020). Following this procedure, we obtained the shapes of primary particles and water-stable aggregates of sizes ranging from 2 to 200 μm (Figure 2a).

To set up the dispersed initial state in our model, we considered a fixed two-dimensional domain with a size of 500 × 500 pixels and a resolution of 2 μm. In this domain, we distributed solid building units with the imaged shapes for a prescribed solid-phase fraction of 35%. This roughly corresponded to a bulk density of 1.3 $g\,cm^{-3}$ when assuming a density of 2.0 $g\,cm^{-3}$ for the primary particles and water-stable microaggregates. Note that the porosity changed over time due to the input and decomposition of POM (Table S3). Based on the shape library, we considered two contrasting soil textures with clay contents of 18% (low clay soil) and 33% (high clay soil).

To account for the heterogeneous distribution of OM explicitly, we assigned reactive edges to the particles. Each of the surface edges of a solid building unit was either marked as reactive or non-reactive. According to the logarithmic decrease of the SSA with mineral particle sizes (Borkovec et al., 1993) and the increasing relative proportion of clay minerals (Fernández-Ugalde et al., 2013, 2016; Schjønning et al., 1999), we assigned the permanent reactive edges of solid building units depending on their size: 10% of the surface was reactive for sand-sized particles (>63 μm), 25% for coarse silt-sized

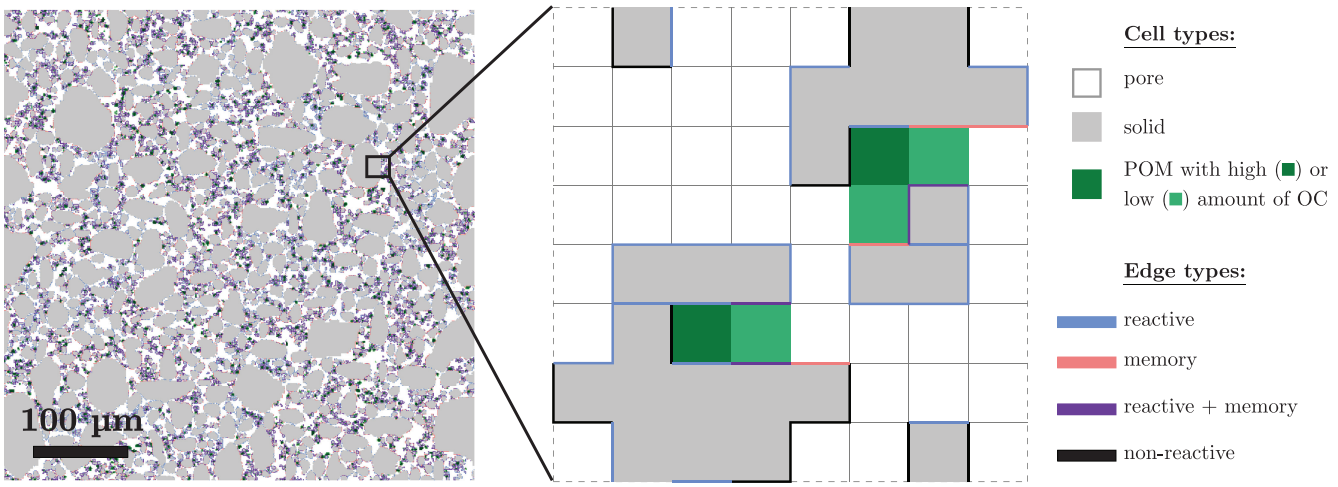

FIGURE 1 Schematic representation (right) of the computational domain (left) with pixels of type solid (■), pore (□) or particulate organic matter (POM) with high (■) or low (■) amount of organic carbon (OC) and edges of type reactive (|), non-reactive (|), memory (|) or both reactive and memory (|).

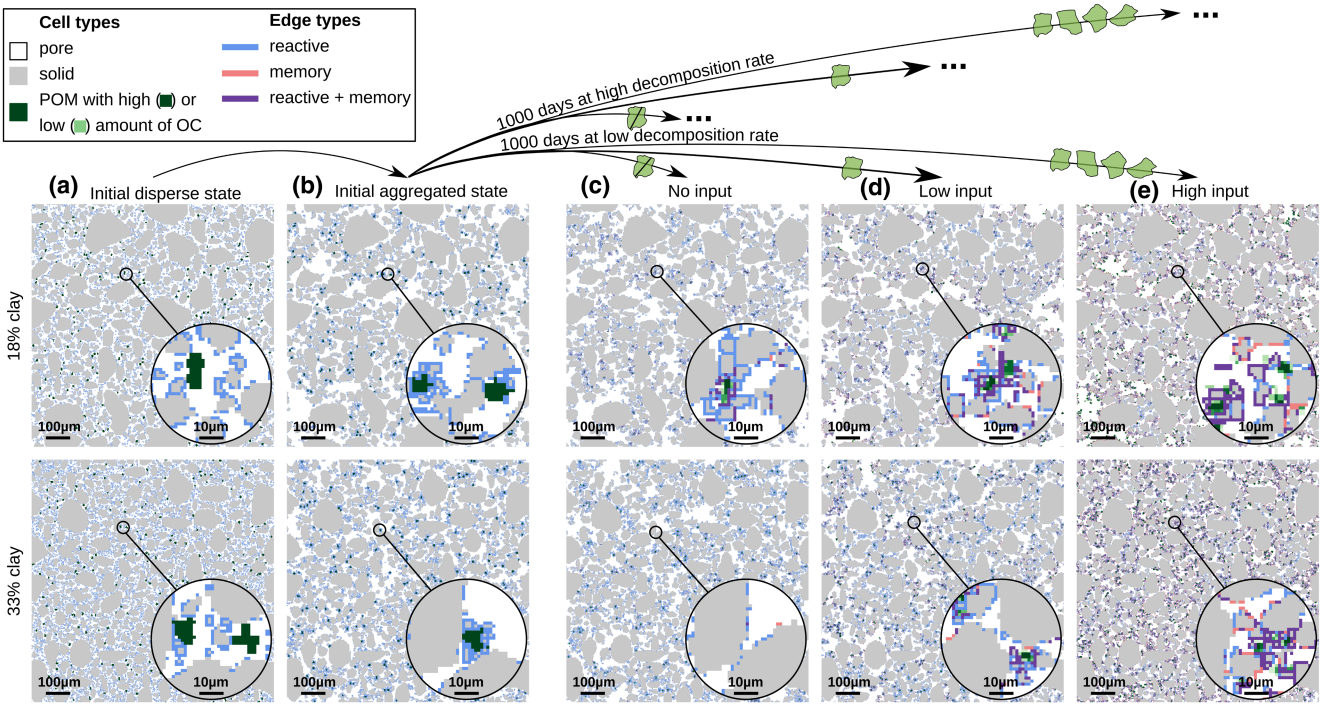

FIGURE 2 Conceptual overview over modeled scenarios and exemplary states (i.e. one repetition each) for different steps of the model, both soil textures and varying input scenarios: Random initial disperse state with shapes from dynamic image analysis (a), aggregated initial state after application of the cellular automaton method (CAM) (b), final state after no input (c), low input (d), and high input (e) scenario.

(>20 µm, <63 µm), 50% for medium silt-sized (>6.3 µm, <20 µm), and 100% of the surface for fine silt and clay-sized particles (<6.3 µm). These reactive edges provided two functions: Firstly, they contributed to the aggregate formation by enabling the aggregation of solid building units with each other and offering attractive spots on the surface for the allocation of POM (Section 2.3). Secondly, they interact with POM and change their surface types since we assumed decomposition to take place after the rapid establishment of contact with a reactive mineral surface (Section 2.4).

We finally added POM particles amounting to 2% of the solid area with sizes constrained to minimum Feret diameters of 6–10 µm according to the prevailing pore diameters in the same range. The initial porosity was reduced from 35% to 33.7% due to the addition of POM. Assuming a POM density of 1.2 $g\,cm^{-3}$ (according to Christensen, 1992) and solid density of 2.65 $g\,cm^{-3}$, the density of quartz, this corresponded to a POM content of 9.01 $mg\,C\,g^{-1}$ and, assuming an OC mass fraction of 40% in POM, a resulting initial amount of 3.60 $mg\,C\,g^{-1}$ as POM-OC. For comparison, OC input of

13 mg C g^{-1} in the form of POM in the sizes <63 μm and 0.63–2 mm were added in incubation experiments by (Bucka et al., 2021). Others added 5–30 mg C g^{-1} (De Gryze et al., 2005), or 5 mg C g^{-1} (Angers & Recous, 1997). Thus, the 2D configurations are based on 3D information from natural soils including the physicochemical properties relevant for the aggregate dynamics.

2.3 | Spatial reorganization of solid phase and POM

The CAM enables the change of the explicit porous structure over time. The CAM rules were based upon the ones described previously (Ray et al., 2017; Rupp et al., 2018, 2019; Zech et al., 2020) for the reorganization of single solid pixels and building units. Compared with these publications, we here applied the CAM for the relocation of building units with realistic shapes based on experimental data and also POM particles and considered the impact of reactive and memory edges.

In every time step, aggregates of solid building units and POM particles, separate solid building units, and POM particles could relocate to achieve the most attractive and stable configuration (Figure S1). Due to the temporal dynamics of POM and surface properties (Section 2.4), the most attractive state could vary over time and the structural reorganization was essential to consider, since it influenced in return the dynamics and turnover of POM, e.g. by occlusion. The range of potential movement was characterized by a stencil, which was higher for small clay particles than that for large aggregates (Rupp et al., 2019; Zech et al., 2020). More precisely, stencil sizes between 10 μm, i.e. 5 pixels, for building units smaller than 100 μm^2 and 2 μm, i.e. 1 pixel, for building units with an area between 1600 and 80,000 μm^2, corresponding to aggregate diameters of approximately 40 and 280 μm, were considered. For larger aggregates the stencil was set to 0. In the simulations, the stencil size was usually large enough to find an attractive spot in one step of the CAM, especially for smaller, mobile building units.

For the relocation of a solid building unit/POM particle or microaggregate, the attractivity of every position within the stencil was evaluated. We considered three different attractive types of contacts between solid building units and POM particles in increasing order of attractivity: solid–solid contacts via reactive surface edges or memory edges, contacts of POM to reactive solid edges, and contacts of POM to solid via memory edges. This hierarchy represented a strong gluing capacity of microbially produced agents. Other types of contacts were disregarded for the calculation of the attractivity.

Additionally, we included a mechanism that allowed for random break-up of structures, depending on the stability represented by the type of contact. At every time step, we checked the current types of contact for every solid building unit/POM particle/aggregate. With a certain probability depending on the contact type, we then moved it randomly, ignoring the attractiveness within the stencil. We considered contacts of POM to memory edges the most stable and set the probability of random moving/breaking-up to 5%, if the POM or solid building unit had at least one POM-memory edge contact. For less stable POM-reactive edge contacts, the probability was 10% and for all other types of contacts, including reactive solid–solid contacts, it was 25%. A higher probability of solid–solid binding spots breaking-up is based on an analysis of dry-sieved aggregate size fractions <250 μm that contained more primary particles within aggregates that were lost in comparison with wet-sieved fractions <250 μm, indicating that OM-mediated binding spots could resist stronger dispersion treatment (Felde et al., 2020).

We applied these CAM rules first to the dispersed initial state (Section 2.2) to get an aggregated initial state potentially leading to occlusions of POM within the microaggregate (Section 3.1).

2.4 | Decomposition and input of POM and simultaneous surface alteration

Starting from the aggregated initial state, we applied a combination of the CAM for the structural reorganization as outlined in Section 2.3 with a model describing the decomposition of POM and simultaneous spreading of microbially produced gluing agents on the solid surface. The initial OC concentration within every POM pixel was 0.48 g C cm^{-3}. We assumed that POM particles are degraded with a first-order rate, similar as in Portell et al. (2018), by an immobile microbial population on the reactive/memory solid edges, which was not modeled explicitly. Our simulations revealed that the share of completely free POM particles was very low at any given time step (<3% for low clay soil, <1% for high clay soil) and the vast majority of POM particles quickly came into physical contact with solid surfaces. Therefore, we did not consider enzymatic degradation of free POM particles without surface interactions as a crucial process in our model and omitted it. For the constant rate coefficient k_{POM}, we considered two variants throughout the simulations. Bucka et al. (2019) measured a C loss of 25% after 30 days for the decomposition of hay litter in an incubation experiment. Assuming an exponential decay, we calculated the "low decomposition rate" $k_{POM} = 0.0096\ day^{-1}$. In an incubation experiment with maize, Recous et al. (1995) measured a C loss of 35% after 18 days, corresponding analogously to the "high decomposition rate" $k_{POM} = 0.0239\ day^{-1}$. We considered different scenarios with these decomposition rates to investigate their impact on the carbon and aggregate turnover (Section 2.5). The rates were further modified depending on the spatial structure and properties of the soil as explained in the following.

Our approach took into account that the POM decomposition depends on the surface that POM particles share with the pore space due to the necessity of oxygen accessibility. This led to a heterogeneous degradation of the POM particle from the outside to the inside. Moreover, the more occluded a POM particle was, the slower it degraded. In the extreme case of complete occlusion, it did not decompose at all. However, note that with the CAM rules described in Section 2.3, a solid building unit could detach from a POM particle and vice versa, if this led to a more attractive configuration.

Additionally, we included a mechanism that allows for random breaking up of structures. Thus, a POM particle that was completely occluded at one time step could get less occluded later, and then decomposed. Finally, if the OC concentration in one POM pixel was zero, its state changed from POM to pore.

When a POM particle was degraded, i.e. as the OC concentration was decaying, part of its OC was released as CO_2-C, and the remainder was taken up by a simultaneously created microbially produced gluing agent on the solid surface with an associated OC concentration. The OC was first taken up on the solid surfaces edges to which the particle was attached in a proportion depending on the carbon use efficiency (CUE). We considered the carbon use efficiency CUE = 0.45, according to the CENTURY model for below-ground OM decomposition (Manzoni et al., 2012). If the OC concentration of the gluing agent at one edge exceeded a maximum concentration equal to the initial and thus maximum OC concentration in POM (=0.48 g C cm^{-3}), the excess concentration was pushed to an adjacent edge. If the concentration at the adjacent edge exceeded the maximum concentration, this procedure was repeated until no agent concentration exceeded the maximum. Thus the agent could spread on the solid surface. On the other hand, the agent was assumed to decay following a first-order rate k_{agent}, which was assumed to be higher than k_{POM} by a factor of 1.5 (Swift et al., 1979).

At solid edges where the agent concentration exceeded a minimum threshold of 1% of the initial OC concentration in a POM pixel (0.0048 g C cm^{-3}), a memory edge was created. As described in Section 2.3, we considered these memory edges the most attractive and stable for the aggregate formation. If the OC concentration of an agent at a memory edge decreased and fell below the minimum threshold, the property as a memory edge was maintained, but its age was increased. Memory edges older than an age of 50 days were then randomly removed with a probability of 0.2% due to an assumed aging process which may lead to the loss of attractive surface properties.

At specified time steps, new POM input was given into the system. This was done by placing POM particles at random positions in the pore space (Section 2.5). The workflow of the simulations, starting from the initial disperse state, generating the initial aggregated state, and then performing the different input scenarios is illustrated in Figure S2.

2.5 | Modeled scenarios

All simulations were carried out for two clay contents namely 18% and 33% using the different experimentally measured particle distributions and resulting surface properties to study the influence of the texture on OM turnover and aggregation. For representativeness, we created 10 repetitions of the initial dispersed state as described in Section 2.2 as a first step, with different shapes of the solid building units and POM particles and different random initial positions. These initial states slightly varied in solid surface, SSA, reactive surface, and proportion of reactive edges (Table S1). On these dispersed initial states, we applied the CAM as described in Section 2.3 until a quasi-stationary state was reached to create aggregated initial states and study the initial aggregate formation (Section 3.1).

We further studied the interplay between aggregate formation and OM turnover by applying the combination of CAM, POM decomposition, and surface alteration as introduced in Section 2.4 on the initial aggregate states for both textures. To investigate the impact of the inherent POM decomposition rate, which can vary e.g. due to different ambient temperatures, we considered two values for the POM decomposition rate (high vs. low, Section 2.4 and Table S4). Additionally, we considered three distinct settings with regard to the new POM input (high vs. low vs. no input, Table S4) to further investigate POM and aggregate turnover dynamics. In the setting without new input, no POM input was given over the modeled time frame, besides the POM that had been placed before the initial aggregate formation process. In the "low" and "high" input scenario, we added four POM particles with an area of 60 μm^2 every 10 or 2 days, respectively. Over the entire simulation time, this amounted to total POM inputs with an OC amount of 6.7 mg C g^{-1} (low input) and 33.3 mg C g^{-1} (high input) in relation to the initial bulk mass. This corresponds to modeled annual OC input rates of 2.4 mg C g^{-1} (low input) and 11.9 mg g^{-1} (high input) reflecting OC input rates analyzed in previous studies (Blanco-Canqui & Lal, 2007; Poirier et al., 2013; Xu et al., 2020). The OC input equals additions of 185% and 925% of the initial amount of OC of 3.60 mg g^{-1}. In total, these scenarios resulted in 120 CAM simulations over 1000 days with a time step of 1 day.

3 | RESULTS

3.1 | Initial aggregate formation

To set up the initial dispersed state starting from the size distributions and shapes of the experimental data of the wet-sieved soil fractions, we first applied the procedure outlined in Section 2.2 for both clay contents (Figure 2a). Comparing the two soil textures, the number of aggregates was initially 71% higher for the high clay soil compared with the low clay soil (Table S2). Correspondingly, the smaller median diameter of aggregates for the high clay soil (38 μm vs. 51 μm for the low clay soil, Figure 3a) mainly reflected the difference in the prescribed size distribution due to the higher proportion of clay particles. Regarding surface properties of the initial states, the total length of the solid surface and thus the SSA were 42% higher for the high clay soil, the total length of the reactive surface was 69% higher, and the percentage of the total reactive surface area was 18% higher (Table S1).

The application of the CAM as described in Section 2.3 resulted in an aggregated initial soil structure. Larger aggregates of POM and solid building units were evident in the aggregated states (Figure 2b), where POM particles were attached to reactive surface sites of the solid phase and solid building units were connected via reactive surfaces. After the development of larger aggregates, the difference in aggregate sizes between the two clay contents was slightly reversed

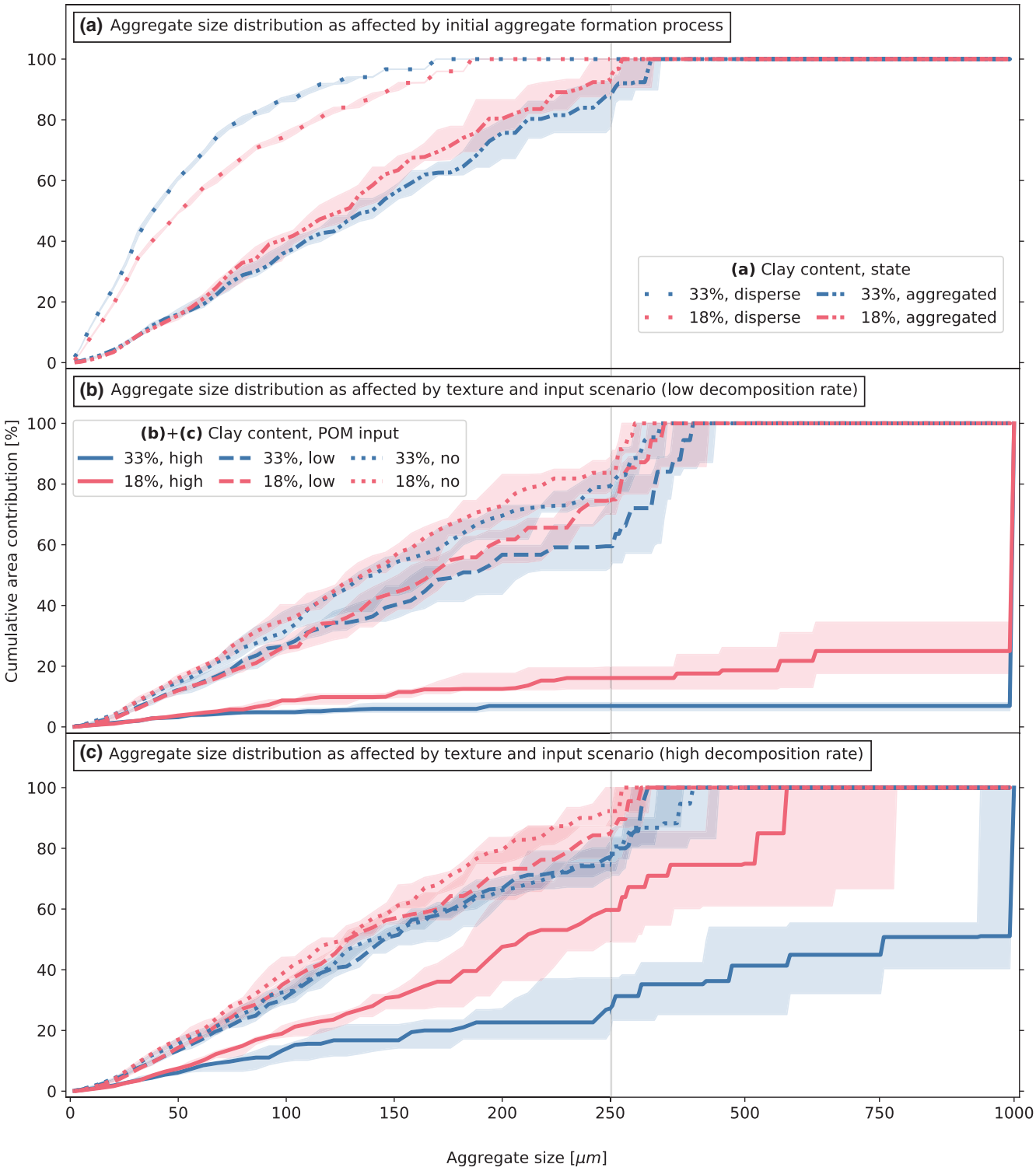

FIGURE 3 Cumulative aggregate size distribution as affected by initial aggregate formation process and different input scenarios with two decomposition rates: Comparison of initial disperse state and aggregated initial state (a), high/low/no input scenarios with low particulate organic matter (POM) decomposition rate (b) and high POM decomposition rate (c). Median of 10 repetitions with error band representing lower and upper quartile.

(Figure 3a). The median aggregate diameter increased from 51 to 126 μm for the low clay soil and from 38 to 140 μm for the high clay soil and the number of aggregates decreased accordingly (Table S2).

The attachment process where POM attached to reactive surfaces of the solid phase and solid particles aggregated with one another is reflected in the total surface coverage by POM and solid, which

increased from 9.9% to 27.4% for the low clay soil and from 15.5% to 36.5% for the high clay soil (Table S1).

3.2 | Aggregate size distribution

On the initial aggregated state (Section 3.1), we applied the combination of methods outlined in Sections 2.3 and 2.4 for three scenarios with varying amounts of POM input and two different POM decomposition rates as described in Section 2.5. The evolutions show that for both clay contents, higher POM input led to larger aggregates, smaller pores, and an increased number of memory edges (pink and violet in Figure 2).

In case of the low decomposition rates, the addition of POM in a low amount only led to a slight increase in the aggregate sizes (Figure 3b). The high POM input, however, led to a significant increase in the aggregate sizes (Figure 3b). Large aggregates of diameter up to 1000 μm representing more than 90% of the total bulk area developed (Figure 3b). Slightly larger aggregates for the high clay soil are evident in the no and low input scenarios (Figure 3b). In the high input setting, the largest aggregates of 1000 μm diameter contributed to a higher share of the total bulk area for the high clay soil (93.1% for high clay soil, 75.0% for the low clay soil, Figure 3b). For all input scenarios, the number of aggregates decreased over time compared with the initial aggregated state (Table S2). Generally, a higher POM input led to fewer but larger aggregates.

In case of high POM decomposition rates, neither of the scenarios without or with low input led to a significant increase in aggregate sizes in course of the simulations (Figure 3c). For the high input, large aggregates developed with diameters up to 578 μm (15.1% area proportion) for the low clay soil, and 1000 μm (48.9% area proportion) for the high clay soil (Figure 3c). Thus, high input led to an increase in aggregate diameters, but compared with the low decomposition rate setting, the aggregates were smaller.

3.3 | POM dynamics

We investigated the dynamics of the amount of OC in POM and the respired CO_2 in response to the different input scenarios. The model allows to elucidate the evolution of the OC including its age since addition to the soil. First, we considered low POM decomposition rates (Figure 4). Although POM was added continuously in the high and low input scenarios, the amount OC in POM in the system did not increase monotonously but rather approached an equilibrium, for high input with both textures and low input with 33% clay (Figure 4a,b,d). Only in the low input setting with 18% clay and the scenarios without additional input, the POM concentration decreased continuously over time (Figure 4c,e,f). When considering high decomposition rates, the OC concentration of POM was lower in every setting (Figure 5). Only in the high input scenarios, the OC concentration increased initially between 0 and 200 days before slightly decreasing (Figure 5a,b). In contrast, it decreased continuously in the low POM input scenarios (Figure 5c,d) and did not tend toward an equilibrium value in the considered time frame. A similar decrease over the whole simulation is apparent without new input of POM (Figure 5e,f).

Comparing the two soil textures, higher OC concentrations of POM occurred at every time step for the high clay soil, for both decomposition rates and all three input regimes. For low POM decomposition rate and high input, e.g. the concentration of POM after 1000 days amounted to 10.4 mg OC g^{-1} bulk for 33% clay compared with 7.5 for 18% clay. Generally, for higher input a larger amount of OC was retained in POM (e.g. for low decomposition rate, 33% clay, 10.4 mg OC g^{-1} for high input, 4.4 mg OC g^{-1} for low input, 1.9 mg OC g^{-1} for no input).

A higher total CO_2 production was obtained for the low clay soil (black arrows in Figures 4 and 5). The increased cumulative CO_2 output for high decomposition rates mainly reflected the decreased amount of OC in POM, besides a small decrease in the amount of OC in the gluing agent. While higher input led to higher amounts of OC in POM, it also led to higher total CO_2 production, e.g. for 33% clay, 25 mg CO_2-C g^{-1} was respired after 1000 days in the high input scenario, compared with 6 mg CO_2-C g^{-1} in the low input scenario and 2 mg CO_2-C g^{-1} in the no input scenario (black arrows in Figure 4).

While total CO_2 outputs varied depending on clay content, CO_2 production rates almost evened out over time. Comparing the two soil textures for low decomposition rates and high input, the CO_2 production rate averaged over the first 200 days was increased by 50% for the low clay soil compared with the high clay soil (15 vs. 10 μg CO_2-C g^{-1} day^{-1}, Figure 4a,b). In the last 200 days, the CO_2 production rate was almost similar between low and high clay soils (approximately 33 μg CO_2-C g^{-1} day^{-1}, Figures 4 and 5a,b). Similarly, the CO_2 production rates compared for the two decomposition rates approached each other.

Starting from similar initial states, the three different input scenarios revealed different OC dynamics in differently aged POM fractions, i.e. fractions of POM added before the initial aggregate formation process (time 0), between 1 and 200 days, 201 and 400 days etc. (Figures 4 and 5). It is evident that in the high input scenarios, the youngest POM fraction accounted for the largest proportion of the total amount of OC at every time step (Figures 4a,b and 5a,b).

Comparing the fate of POM that was added at time step zero (dark blue bars in Figures 4 and 5), a higher additional POM input led to higher decomposition of this oldest fraction. In case of the low decomposition rates and high clay soil, an OC content of 1.9 mg g^{-1} (equivalent to a share of 51.7%) of the old POM fraction remained after 1000 days when no POM was added (Figure 4f), while only a concentration of 1.5 mg g^{-1} (equivalent to 42.9%) remained in the low input scenario (Figure 4d) and 0.7 mg g^{-1} (equivalent to 19.8%) in the high input scenario (Figure 4b). A similar decrease in the amount of OC of the oldest POM fraction for higher input was observed for the low clay soil (Figure 4a,c,e), and also for both soil textures and high decomposition rates (Figure 5). Because the total POM input after the initially placed POM varied between the three input settings, we did not consider a comparison of absolute OC contents for the other POM age fractions.

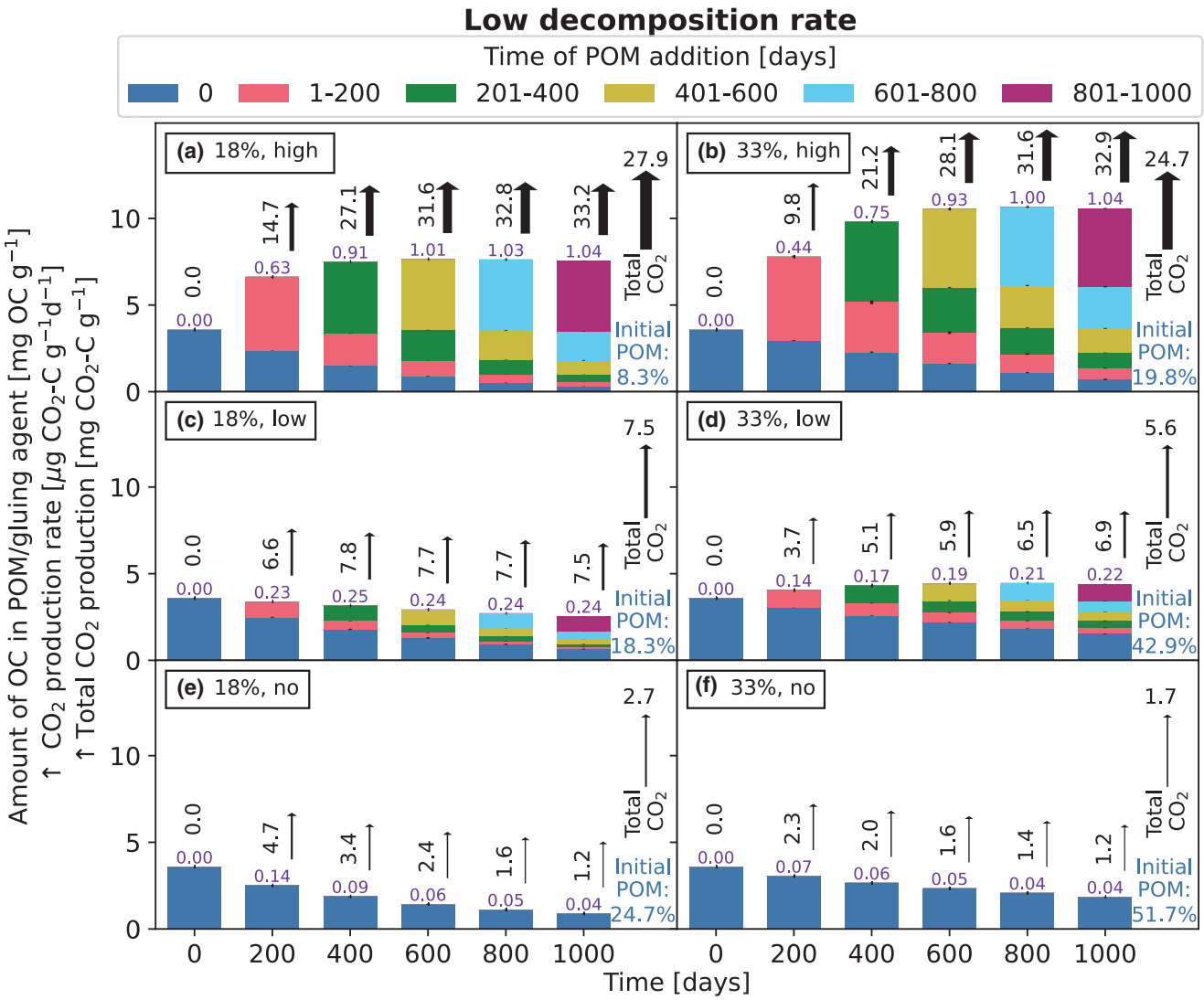

FIGURE 4 Amount of organic carbon (OC) in different fractions of particulate organic matter (POM) by age (differently colored bars) and gluing agent (number above bar), CO_2 production rate (arrows above bars), total CO_2 production (rightmost arrows), and remaining share of initial POM in different input scenarios and for both soil textures with low decomposition rate: High/low/no input scenarios for low clay soil (a, c, e) and high clay soil (b, d, f). Median of 10 repetitions with error bars representing lower and upper quartile.

When comparing the relative proportion of the amount of OC of the respective added POM age fraction, we observed that higher input also led to higher decomposition compared with the low input scenario, although to a lesser degree. For instance, in case of low decomposition rates and the high clay soil, 73% of the OC in the POM fraction that was added between 1 and 200 days was still present after 200 days in the high input scenario, while 77% was present in the low input setting (Figure 4). Similar observations hold true for the high decomposition rates.

3.4 | Surface dynamics

For both decomposition rates, higher input led to higher coverage of the solid surface by POM (Figure 6a,b). Starting with a surface coverage by POM of 5.0% for the low clay soil and 4.1% for the high clay soil, the surface coverage increased to 20.9% for both soils in the high input scenario and to 8.4% and 8.8% in the low input scenario, while it decreased to 3.7% and 3.9% without new input for the low decomposition rate. Note that while the total solid surface area, reactive surface area, and share of reactive surface area differed for the two textures (Section 3.1 and Figure 6c,d), the surface coverage by POM almost coincided.

Surface coverage by POM and solid building units was higher for the high clay soil for both decomposition rates and all input regimes (blue curves in Figure 6c,d). While it increased for high input and 18% clay, e.g. for low decomposition rates from 27.4% to 34.7%, it increased less for the high clay soil, from 36.5% to 38.7%. For the high decomposition rates, it only increased significantly for the low clay soil (Figure 6d).

Since there were no memory edges in the initial state, the amount of memory edges increased in all scenarios, up to a share of the total surface of 52.1% (Figure 6e,f). In the scenarios without POM input and the low input scenario for the low clay soil and high decomposition rate,

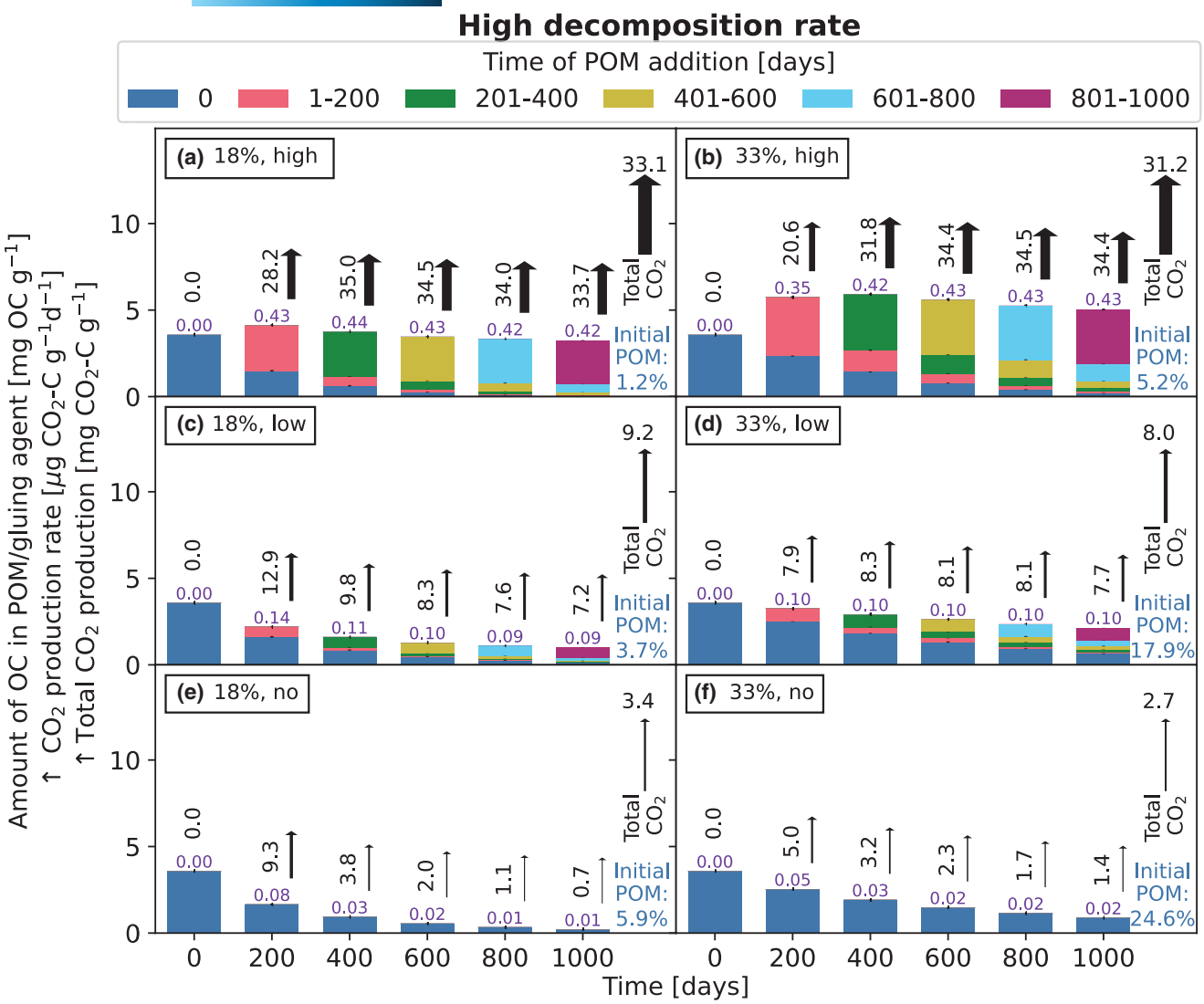

FIGURE 5 Amount of organic carbon (OC) in different fractions of particulate organic matter (POM) by age (differently colored bars) and gluing agent (number above bar), CO_2 production rate (arrows above bars), total CO_2 production (rightmost arrows), and remaining share of initial POM in different input scenarios and for both soil textures with high decomposition rate: High/low/no input scenarios for low clay soil (a, c, e) and high clay soil (b, d, f). Median of 10 repetitions with error bars representing lower and upper quartile.

the share of the surface that was marked as memory edges increased initially, but decreased toward the end of the simulation time (Figure 6e,f). Generally, higher input led to higher amounts of memory edges. The low clay soil exhibited a higher amount of memory edges at the beginning of the simulations, but the differences balanced out or even reversed in case of the high input settings toward the end time (Figure 6e,f).

4 | DISCUSSION

4.1 | Advantages of the dynamic and spatially explicit modeling approach

Our spatially and temporally explicit dynamic model enables novel insights into the interplay of changing soil structure, the turnover of POM, and simultaneous modulation of soil surface properties that influence aggregation. As anticipated by Pot et al. (2021), our approach allows to include and analyze the influence of the spatial configuration and interaction of pore space, soil particles, and POM in a mechanistic way, for the first time adapted from image-based, experimental data of aggregate size distributions and shapes—in contrast to macroscale, lumped parameter, or compartment models. We did not use any fitted parameters. Rather, the results were obtained by forward simulations based on justified assumptions on mechanisms, model components, and parameters yielding a basis for the study and interpretation of further scenarios. Keeping the assumptions made in mind, we have, e.g., access to the distribution of POM of different ages under the varying conditions of the scenarios. The spatially explicit and dynamic representation of pores and particles allows to study the aggregate turnover as a function of access of reactive surfaces to the pore space. This enables us to distinguish occluded structures

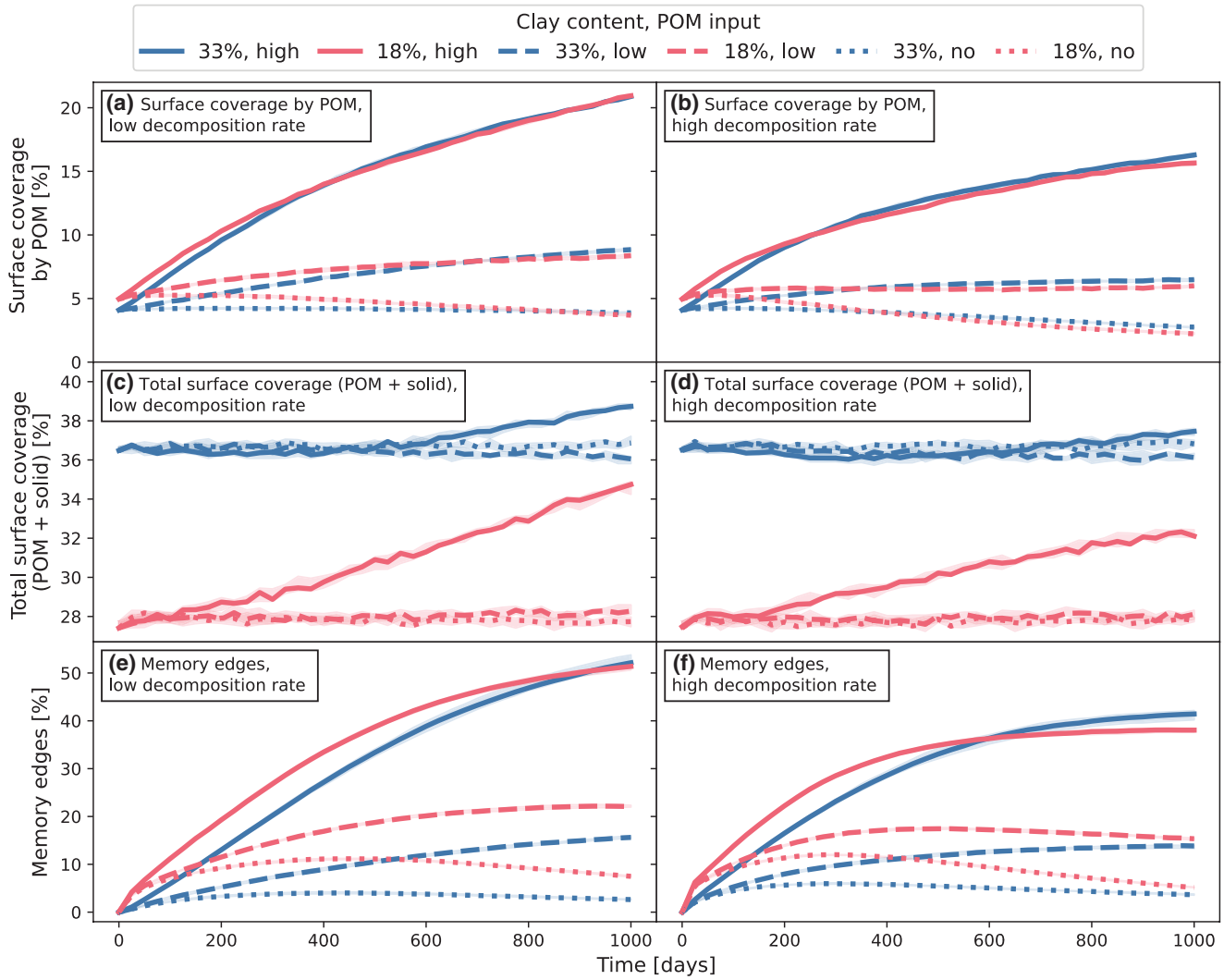

FIGURE 6 Surface coverage by particulate organic matter (POM) (a, b) and solid + POM (c, d) and proportion of solid surface that is marked as memory edges (e, f) over time in input scenarios with low (a, c, e) and high (b, d, f) POM decomposition rate. Median of 10 repetitions with error band representing lower and upper quartiles.

from freely accessible ones and analyze mechanisms related to soil carbon destabilization (Bailey et al., 2019). The influence of OM input on structure evolution, aggregate size, and CO_2 production at the pore scale was quantified, and led to the emergence of dynamic equilibria under different conditions.

4.2 | Soil aggregate dynamics outweigh texture effects at low OM decomposition rate

We quantified the modeled aggregate size distribution, induced by different POM input scenarios comparing different soil textures ('low clay' 18% and 'high clay soil' with 33% clay content) (Figures 2 and 3). In the different scenarios, where either a high amount, low amount, or no POM was added continuously, higher input stimulated the aggregation mechanism, i.e. led to larger aggregate sizes up to 1000 µm (Figure 3b). The higher abundance of fine mineral particles in the high clay soil caused smaller particle sizes in the initial dispersed states, but after POM addition, the initially formed aggregates in the high clay soil were larger or of similar size compared with the aggregates in the low clay soil for all different input scenarios (Figure 3).

The aggregation in this case was largely determined by the POM input and mostly decoupled from the soil texture. This confirms a similar result of POM inducing the formation of large macroaggregates, independent of texture, found in an incubation experiment (Bucka et al., 2021). This implies that the POM-induced aggregate formation can connect particles of all sizes and underlines that also sand grains can be found within aggregates and thus contribute to a larger size of aggregates (Bucka et al., 2021; Felde et al., 2020; Paradiś et al., 2017).

Global change leads to climate-driven increase of soil temperatures (Soong et al., 2020) resulting in raised decomposition rates of OC (Davidson & Janssens, 2006; Kirschbaum, 1995). An increase of 150% in our model induced smaller soil aggregates indicating that the balance between POM decomposition and its stabilization

through aggregation and occlusion shifts toward decomposition, i.e. more POM is decomposed before being possibly occluded within aggregates. For both soil textures, we observed similar aggregate size distributions for the no and low input scenarios. In contrast to the scenarios with low decomposition rate, the low amount of POM input was insufficient to induce aggregate formation and the aggregate breakdown prevailed. This indicates that with increasing decomposition rates, an increase in POM input is necessary such that large aggregates are formed. A high input resulted in larger aggregates for the high clay content soil (Figure 3c), and the difference in aggregate sizes between clay contents was even greater than for the low decomposition rate. The impact of fine mineral particles that comprise more reactive surfaces may explain the build-up of larger aggregates which could induce a higher persistence of the POM in the high clay soils through their occlusion.

Our results suggest that the POM input rate outweighs the texture effect on large aggregate formation at low POM decomposition rate. At a high POM decomposition rate, both texture and POM input significantly affect the formation of large aggregates. The higher soil clay content enhanced the aggregate formation here, because the formation of large aggregates relies on the interaction with mineral surfaces leading to POM occlusion, preventing a rapid POM decomposition

4.3 | Structural re-arrangement induces dynamic changes of POM storage

Particulate organic matter was decomposed mostly depending on the individual surface interactions with solid building units, i.e. primary particles and soil aggregates. The development of the POM-C over time is therefore influenced by soil texture and the dynamic re-arrangement of soil structures around them. Although POM was added continuously in the high and low input scenarios, the amount of POM remained at a constant level toward the end of the simulation. For the high POM input scenario (at low decomposition), the POM amount reached a plateau that was higher than the initial value, and highest in the high clay soil (Figure 4a,b). For the low POM input scenario, the amount of OC in POM increased only in case of the high clay soil and the low decomposition rate, but decreased in all other settings, suggesting that the higher available surface area in the high clay soils is necessary for OC storage at low POM input scenarios (Figures 4c,d and 5c,d). This reflects the results of a previous experimental study of a clay content gradient in an agricultural soil where the OM storage in terms of POM increased with clay content (Schweizer et al., 2021).

The POM input had a major effect that was stronger than the different soil textures (Figures 4 and 5). This indicates that the storage of OC is mainly driven by input and the resulting re-arrangement of aggregates. However, there is still a less pronounced influence of the soil texture which can switch from a decrease of POM to an increase over time under the low POM input regime and the low decomposition rate (Figure 4c,d). This calls for a more careful evaluation of the role of clay content for OC dynamics under elevated decomposition rates, e.g. caused by elevated temperatures due to climate change. A higher clay content can support OC sequestration probably only at low decomposition rates. At higher decomposition rates, the surface interaction and occlusion processes may slow down but not prevent the net loss of OC.

For both decomposition rates, an increase in POM input led to an increased mineralization of old, i.e. initially present POM. This was indicated by the proportions of initial POM that decreased when the POM input increased (Figures 4 and 5). The occlusion of this initial POM within aggregates was increasingly affected by the re-arrangement of the soil structure driven by the POM input. This means that a higher input of POM led to a higher break-up of aggregate structures and loss of old POM occlusion. The break-up of old POM occlusion is related to weaker gluing effects when an aggregate associates with a newly added POM forming a stronger bonding elsewhere. This suggests that the input of POM stimulates aggregate turnover resulting in an increased mineralization of the previously occluded POM and the integration and occlusion of fresh POM into newly formed aggregates. This could explain the primed decomposition of old POM through a re-arrangement of the soil structure as freshly developed gluing agents lead to a divergent stabilization region in the aggregates.

The possibility for such a detailed investigation is one main advantage of our spatially and temporally explicit modeling approach compared with experimental studies, since in soils, the localization of OM during turnover processes is very difficult to assess and visualize (Peth et al., 2014).

4.4 | Surface effects explain structural priming and texture influence on POM dynamics

Permanent reactive surfaces and temporary OM coated mineral edges on the solid surface formed through the turnover of POM are key components for the enhancement of aggregate structures and the occlusion of POM. The temporarily limited effect of OM-coated mineral edges marks their effect as so-called memory edges of locally decomposed POM on the surrounding mineral matrix. Such memory edges, which are derived from POM decomposition, cause a sustained enhancement of surface reactivity as related to altered organo–mineral interfaces (Kleber et al., 2021).

Since fine mineral particles have a large SSA and a high proportion of reactive surface, the high clay soil had a higher total solid surface area and percentage of reactive surface area (Table S1). The input of POM led to an increase in surface coverage, without covering the entire reactive surface, even in the high input setting (Figure 6; Table S2). The POM content leveled off approaching a dynamic equilibrium without having achieved a complete coverage of the reactive surface. Additional simulations with doubled and tripled amounts of POM input and longer running time showed that surface coverages turned stationary at times <3000 days, but at correspondingly higher levels (Figure S3). Surface coverage by POM

however never reached 60% in either scenario. This means that not all mineral surfaces were associated with POM which directly couples the POM turnover with the observed structural dynamics. Accordingly, the structural re-arrangement may influence the distribution and organo–mineral interactions of POM processing into dissolved OM at the microscale (Schlüter et al., 2022).

For both clay contents, the surface coverage by POM was very similar in all scenarios (Figure 6a,b). Since the high clay soil exhibited a larger total surface area (Table S1), this means that a larger total part of the surface area was covered by POM for the high clay soil and consequently, a higher proportion of the POM surface area was covered by solid building units. This supports the increase in the amount of OC in high clay soil outlined in Section 4.2 due to a higher occlusion of POM. In contrast, the surface coverage by POM and solid combined was higher for the high clay soil. This indicates that aggregation between solid particles via reactive edges increased in the high clay texture, which was due to the higher proportion of fine clay particles with a high proportion of reactive edges.

Comparing the temporal development of surface coverage by POM and surface coverage by POM and solid helps to illuminate the aggregate formation process and inclusion of fresh POM. For both soil textures, the increase in surface coverage by POM was larger than the increase in surface coverage by solid and POM combined. This indicates that the aggregate formation and occlusion of new POM was not solely due to POM particles attaching at free solid surface spots and acting as connecting solid building units. Rather, less stable solid–solid connections broke up and were replaced by more stable POM–solid connections. This seemed to be especially the case for the high clay soil, where the higher amount of fine clay minerals resulted in more solid–solid connections, which then were increasingly replaced with high POM input. The break-up and formation of new POM-mineral structures, stimulated by a high input, confirms the observed structural priming effects in Section 4.2, where high input led to higher mineralization of old POM.

In conclusion, our results show that the dynamic re-arrangement of soil structure is an important process driving POM-related turnover of carbon in soils (Figure 7). Our model approach enabled insights into underlying interactions of aggregate formation and break-down, OC turnover, and the role of organo–mineral surface interactions that could not be quantified with experimental approaches. Our results revealed that POM input can outweigh texture effects on aggregate dynamics

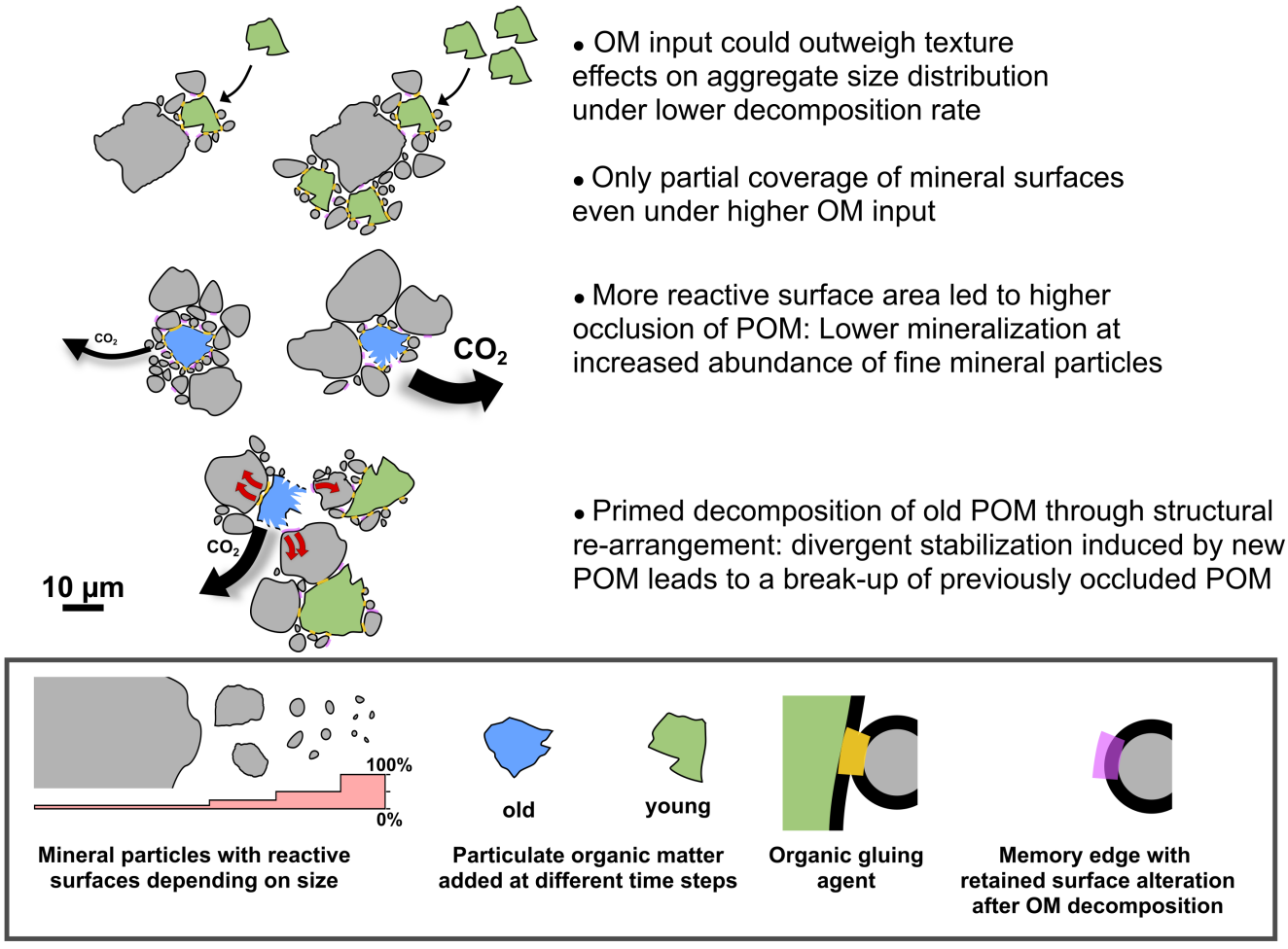

FIGURE 7 Graphical conclusion.

at lower decomposition rate. An increased decomposition led to higher turnover of POM into CO_2 in low clay soils, whereas this effect was counteracted in high clay soils due to increased surface interactions. Texture also shifted the temporal dynamics: Low clay soils usually resulted in lower occlusion leading to a quick increase of CO_2 and OM gluing agent production, which approximated the final results of the high clay soils showing a delayed response. The primed decomposition of old POM induced by fresh POM input could be explained through the dynamic structural rearrangement: The stabilization of individual particles through gluing joints and divergent movement led to a break-up of old gluing joints and the subsequent decomposition of the attached POM. Our modeling approach warrants further studies to implement the dynamic re-arrangement of soil structure into the prediction of carbon storage and extend toward biogeochemically more heterogeneous structures of organic and mineral components also including a more heterogeneous supply of POM. Finally, the mutual feedback from new laboratory and simulation experiments will foster the understanding of the underlying processes. For example, incubation studies with different POM input scenarios and the subsequent analysis of aggregate structures, or isotope studies revealing the age of different OM fractions can be related to the presented results.

ACKNOWLEDGMENTS

We gratefully acknowledge financial support of the Deutsche Forschungsgemeinschaft (DFG) within the framework of the research unit 2179 "MAD Soil – Microaggregates: Formation and turnover of the structural building blocks of soils," projects 251268514, 276972051 and 276973106. We thank F. Lang and G. Kayser (both University of Freiburg) for the provision of the particle and aggregate shapes based on dynamic image analysis using a QICPIC machine as published in previous works. The authors would like to thank two anonymous reviewers for their evaluation of the manuscript and their very thoughtful comments and constructive feedback, which helped us to improve the manuscript. Open Access funding enabled and organized by Projekt DEAL.

CONFLICTS OF INTEREST

The authors declare that they have no conflict of interest.

DATA AVAILABILITY STATEMENT

The data that support the findings of this study are openly available in figshare at https://doi.org/10.6084/m9.figshare.19663986 (Zech, Schweizer, et al., 2022).

ORCID

Simon Zech https://orcid.org/0000-0002-0475-2651
Steffen A. Schweizer https://orcid.org/0000-0002-9489-1005
Franziska B. Bucka https://orcid.org/0000-0003-3922-8136
Nadja Ray https://orcid.org/0000-0002-9596-953X
Ingrid Kögel-Knabner https://orcid.org/0000-0002-7216-8326
Alexander Prechtel https://orcid.org/0000-0002-6982-2403

REFERENCES

Amézketa, E. (1999). Soil aggregate stability: A review. *Journal of Sustainable Agriculture*, *14*, 83–151.

Angers, D. A., & Recous, S. (1997). Decomposition of wheat straw and rye residues as affected by particle size. *Plant and Soil*, *189*, 197–203.

Bailey, V. L., Bond-Lamberty, B., DeAngelis, K., Grandy, A. S., Hawkes, C. V., Heckman, K., Lajtha, K., Phillips, R. P., Sulman, B. N., Todd-Brown, K. E. O., & Wallenstein, M. D. (2018). Soil carbon cycling proxies: Understanding their critical role in predicting climate change feedbacks. *Global Change Biology*, *24*, 895–905. https://doi.org/10.1111/gcb.13926

Bailey, V. L., Pries, C. H., & Lajtha, K. (2019). What do we know about soil carbon destabilization? *Environmental Research Letters*, *14*, 083004. https://doi.org/10.1088/1748-9326/ab2c11

Baveye, P. C., Otten, W., Kravchenko, A., Balseiro-Romero, M., Beckers, É., Chalhoub, M., Darnault, C., Eickhorst, T., Garnier, P., Hapca, S., Kiranyaz, S., Monga, O., Mueller, C. W., Nunan, N., Pot, V., Schlüter, S., Schmidt, H., & Vogel, H.-J. (2018). Emergent properties of microbial activity in heterogeneous soil microenvironments: Different research approaches are slowly converging, yet major challenges remain. *Frontiers in Microbiology*, *9*, 1929. https://doi.org/10.3389/fmicb.2018.01929

Blanco-Canqui, H., & Lal, R. (2007). Soil structure and organic carbon relationships following 10 years of wheat straw management in no-till. *Soil and Tillage Research*, *95*, 240–254. https://doi.org/10.1016/j.still.2007.01.004

Borkovec, M., Wu, Q., Degovics, G., Laggner, P., & Sticher, H. (1993). Surface area and size distributions of soil particles. *Colloids and Surface A: Physicochemical and Engineering Aspects*, *73*, 65–76.

Bucka, F. B., Felde, V. J. M. N. L., Peth, S., & Kögel-Knabner, I. (2021). Disentangling the effects of OM quality and soil texture on microbially mediated structure formation in artificial model soils. *Geoderma*, *403*, 115213. https://doi.org/10.1016/j.geoderma.2021.115213

Bucka, F. B., Kölbl, A., Uteau, D., Peth, S., & Kögel-Knabner, I. (2019). Organic matter input determines structure development and aggregate formation in artificial soils. *Geoderma*, *354*, 113881. https://doi.org/10.1016/j.geoderma.2019.113881

Chenu, C., & Jaunet, A. M. (1992). Cryoscanning electron microscopy of microbial extracellular polysaccharides and their association with minerals. *Scanning*, *14*, 360–364. https://doi.org/10.1002/sca.4950140609

Chenu, C., & Stotzky, G. (2002). Interactions between microorganisms and soil particles: An overview. In P. M. Huang, J. M. Bollag, & N. Senesi (Eds.), *Interactions between soil particles and microorganisms: Impact on the terrestrial ecosystem* (pp. 3–40). John Wiley and Sons.

Christensen, B. T. (1992). Physical fractionation of soil and organic matter in primary particle size and density separates. *Advances in Soil Sciences*, *20*, 1–90.

Cotrufo, M. F., Wallenstein, M. D., Boot, C. M., Denef, K., & Paul, E. (2013). The microbial efficiency-matrix stabilization (MEMS) framework integrates plant litter decomposition with soil organic matter stabilization: Do labile plant inputs form stable soil organic matter? *Global Change Biology*, *19*, 988–995. https://doi.org/10.1111/gcb.12113

Crawford, J. W., Deacon, L., Grinev, D., Harris, J. A., Ritz, K., Singh, B. K., & Young, I. (2012). Microbial diversity affects self-organization of the soil-microbe system with consequences for function. *Journal of the Royal Society Interface*, *9*, 1302–1310. https://doi.org/10.1098/rsif.2011.0679

Davidson, E. A., & Janssens, I. A. (2006). Temperature sensitivity of soil carbon decomposition and feedbacks to climate change. *Nature*, *440*, 165–173. https://doi.org/10.1038/nature04514

De Gryze, S., Six, J., Brits, C., & Merckx, R. (2005). A quantification of short-term macroaggregate dynamics: Influences of wheat residue

input and texture. *Soil Biology and Biochemistry*, *37*, 55–66. https://doi.org/10.1016/j.soilbio.2004.07.024

Dufrêne, Y. F., Boonaert, C. J. P., & Rouxhet, P. G. (1999). Surface analysis by X-ray photoelectron spectroscopy in study of bioadhesion and biofilms. In R. J. Doyle (Ed.), *Methods in enzymology* (pp. 375–389). Elsevier. https://doi.org/10.1016/S0076-6879(99)10030-2

Fatichi, S., Or, D., Walko, R., Vereecken, H., Young, M. H., Ghezzehei, T. A., Hengl, T., Kollet, S., Agam, N., & Avissar, R. (2020). Soil structure is an important omission in earth system models. *Nature Communications*, *11*, 522. https://doi.org/10.1038/s41467-020-14411-z

Felde, V. J. M. N. L., Schweizer, S. A., Biesgen, D., Ulbrich, A., Uteau, D., Knief, C., Graf-Rosenfellner, M., Kögel-Knabner, I., & Peth, S. (2020). Wet sieving versus dry crushing: Soil microaggregates reveal different physical structure, bacterial diversity and organic matter composition in a clay gradient. *European Journal of Soil Science*, *72*, 1–19. https://doi.org/10.1111/ejss.13014

Fernández-Ugalde, O., Barré, P., Hubert, F., Virto, I., Girardin, C., Ferrage, E., Caner, L., & Chenu, C. (2013). Clay mineralogy differs qualitatively in aggregate-size classes: Clay-mineral-based evidence for aggregate hierarchy in temperate soils. *European Journal of Soil Science*, *64*, 410–422. https://doi.org/10.1111/ejss.12046

Fernández-Ugalde, O., Barré, P., Virto, I., Hubert, F., Billiou, D., & Chenu, C. (2016). Does phyllosilicate mineralogy explain organic matter stabilization in different particle-size fractions in a 19-year C3/C4 chronosequence in a temperate Cambisol? *Geoderma*, *264*, 171–178. https://doi.org/10.1016/j.geoderma.2015.10.017

Gaillard, V., Chenu, C., Recous, S., & Richard, G. (1999). Carbon, nitrogen and microbial gradients induced by plant residues decomposing in soil. *European Journal of Soil Science*, *50*, 567–578. https://doi.org/10.1046/j.1365-2389.1999.00266.x

Gao, J., Jansen, B., Cerli, C., Helmus, R., Mikutta, R., Dultz, S., Guggenberger, G., & Kalbitz, K. (2017). Competition and surface conditioning alter the adsorption of phenolic and amino acids on soil minerals: Adsorption of phenolic and amino acids on minerals. *European Journal of Soil Science*, *68*, 667–677. https://doi.org/10.1111/ejss.12459

Gao, J., Mikutta, R., Jansen, B., Guggenberger, G., Vogel, C., & Kalbitz, K. (2020). The multilayer model of soil mineral-organic interfaces-a review. *Journal of Plant Nutrition and Soil Science*, *183*, 27–41. https://doi.org/10.1002/jpln.201900530

Golchin, A., Oades, J. M., Skjemstad, J. O., & Clarke, P. (1994). Soil structure and carbon cycling. *Soil Research*, *32*, 1043–1068. https://doi.org/10.1071/SR9941043

Guhra, T., Stolze, K., & Totsche, K. U. (2022). Pathways of biogenically excreted organic matter into soil aggregates. *Soil Biology and Biochemistry*, *164*, 108483. https://doi.org/10.1016/j.soilbio.2021.108483

Hattori, T. (1988). Soil aggregates as microhabitats of microorganisms. *Science Reports of the Research Institutes, Tohoku University, Series D: Agriculture*, *37*, 23–36.

Huang, Q., Wu, H., Cai, P., Fein, J. B., & Chen, W. (2015). Atomic force microscopy measurements of bacterial adhesion and biofilm formation onto clay-sized particles. *Scientific Reports*, *5*, 16857. https://doi.org/10.1038/srep16857

Jastrow, J. D. (1996). Soil aggregate formation and the accrual of particulate and mineral-associated organic matter. *Soil Biology and Biochemistry*, *28*, 665–676. https://doi.org/10.1016/0038-0717(95)00159-X

Jilling, A., Keiluweit, M., Gutknecht, J. L. M., & Grandy, A. S. (2021). Priming mechanisms providing plants and microbes access to mineral-associated organic matter. *Soil Biology and Biochemistry*, *158*, 108265. https://doi.org/10.1016/j.soilbio.2021.108265

Keiluweit, M., Bougoure, J. J., Zeglin, L. H., Myrold, D. D., Weber, P. K., Pett-Ridge, J., Kleber, M., & Nico, P. S. (2012). Nano-scale investigation of the association of microbial nitrogen residues with iron (hydr)oxides in a forest soil O-horizon. *Geochimica et Cosmochimica Acta*, *95*, 213–226. https://doi.org/10.1016/j.gca.2012.07.001

Kirschbaum, M. U. F. (1995). The temperature dependence of soil organic matter decomposition, and the effect of global warming on soil organic C storage. *Soil Biology and Biochemistry*, *27*, 753–760. https://doi.org/10.1016/0038-0717(94)00242-S

Kleber, M., Bourg, I. C., Coward, E. K., Hansel, C. M., Myneni, S. C. B., & Nunan, N. (2021). Dynamic interactions at the mineral–organic matter interface. *Nature Reviews Earth & Environment*, *2*, 402–421. https://doi.org/10.1038/s43017-021-00162-y

Kleber, M., Sollins, P., & Sutton, R. (2007). A conceptual model of organo-mineral interactions in soils: Self-assembly of organic molecular fragments into zonal structures on mineral surfaces. *Biogeochemistry*, *85*, 9–24. https://doi.org/10.1007/s10533-007-9103-5

Kögel-Knabner, I., 2002. The macromolecular organic composition of plant and microbial residues as inputs to soil organic matter. *Soil Biology and Biochemistry 34*, 139–162. https://doi.org/10.1016/S0038-0717(01)00158-4

Lehmann, J., Hansel, C. M., Kaiser, C., Kleber, M., Maher, K., Manzoni, S., Nunan, N., Reichstein, M., Schimel, J. P., Torn, M. S., Wieder, W. R., & Kögel-Knabner, I. (2020). Persistence of soil organic carbon caused by functional complexity. *Nature Geoscience*, *13*, 529–534. https://doi.org/10.1038/s41561-020-0612-3

Liang, J., Zhou, Z., Huo, C., Shi, Z., Cole, J. R., Huang, L., Konstantinidis, K. T., Li, X., Liu, B., Luo, Z., Penton, C. R., Schuur, E. A. G., Tiedje, J. M., Wang, Y.-P., Wu, L., Xia, J., Zhou, J., & Luo, Y. (2018). More replenishment than priming loss of soil organic carbon with additional carbon input. *Nature Communications*, *9*, 3175. https://doi.org/10.1038/s41467-018-05667-7

Manzoni, S., Taylor, P., Richter, A., Porporato, A., & Ågren, G. I. (2012). Environmental and stoichiometric controls on microbial carbon-use efficiency in soils. *The New Phytologist*, *196*, 79–91. https://doi.org/10.1111/j.1469-8137.2012.04225.x

McCarthy, J. F., Ilavsky, J., Jastrow, J. D., Mayer, L. M., Perfect, E., & Zhuang, J. (2008). Protection of organic carbon in soil microaggregates via restructuring of aggregate porosity and filling of pores with accumulating organic matter. *Geochimica et Cosmochimica Acta*, *72*, 4725–4744. https://doi.org/10.1016/j.gca.2008.06.015

Paradiś, A., Brueck, C., Meisenheimer, D., Wanzek, T., & Dragila, M. I. (2017). Sandy soil microaggregates: Rethinking our understanding of hydraulic function. *Vadose Zone Journal*, *16*, 1–10. https://doi.org/10.2136/vzj2017.05.0090

Peth, S., Chenu, C., Leblond, N., Mordhorst, A., Garnier, P., Nunan, N., Pot, V., Ogurreck, M., & Beckmann, F. (2014). Localization of soil organic matter in soil aggregates using synchrotron-based X-ray microtomography. *Soil Biology and Biochemistry*, *78*, 189–194. https://doi.org/10.1016/j.soilbio.2014.07.024

Poirier, V., Angers, D. A., Rochette, P., & Whalen, J. K. (2013). Initial soil organic carbon concentration influences the short-term retention of crop-residue carbon in the fine fraction of a heavy clay soil. *Biology and Fertility of Soils*, *49*, 527–535. https://doi.org/10.1007/s00374-013-0794-6

Portell, X., Pot, V., Garnier, P., Otten, W., & Baveye, P. C. (2018). Microscale heterogeneity of the spatial distribution of organic matter can promote bacterial biodiversity in soils: Insights from computer simulations. *Frontiers in Microbiology*, *9*.

Pot, V., Portell, X., Otten, W., Garnier, P., Monga, O., & Baveye, P. C. (2021). Accounting for soil architecture and microbial dynamics in microscale models: Current practices in soil science and the path ahead. *European Journal of Soil Science*, *73*(1). https://doi.org/10.1111/ejss.13142

Pronk, G. J., Heister, K., & Kögel-Knabner, I. (2013). Is turnover and development of organic matter controlled by mineral composition? *Soil Biology and Biochemistry*, *67*, 235–244. https://doi.org/10.1016/j.soilbio.2013.09.006

Pronk, G. J., Heister, K., Ding, G.-C., Smalla, K., & Kögel-Knabner, I. (2012). Development of biogeochemical interfaces in an artificial soil incubation experiment; aggregation and formation of organo-mineral associations. *Geoderma*, *189–190*, 585–594. https://doi.org/10.1016/j.geoderma.2012.05.020

Rabbi, S. M. F., Minasny, B., McBratney, A. B., & Young, I. M. (2020). Microbial processing of organic matter drives stability and pore geometry of soil aggregates. *Geoderma*, *360*, 114033. https://doi.org/10.1016/j.geoderma.2019.114033

Ray, N., Rupp, A., & Prechtel, A. (2017). Discrete-continuum multiscale model for transport, biomass development and solid restructuring in porous media. *Advances in Water Resources*, *107*, 393–404. https://doi.org/10.1016/j.advwatres.2017.04.001

Recous, S., Robin, D., Darwis, D., & Mary, B. (1995). Soil inorganic N availability: Effect on maize residue decomposition. *Soil Biology and Biochemistry*, *27*, 1529–1538. https://doi.org/10.1016/0038-0717(95)00096-W

Rupp, A., Guhra, T., Meier, A., Prechtel, A., Ritschel, T., Ray, N., & Totsche, K. U. (2019). Application of a cellular automaton method to model the structure formation in soils under saturated conditions: A mechanistic approach. *Frontiers in Environmental Science*, *7*, 170. https://doi.org/10.3389/fenvs.2019.00170

Rupp, A., Totsche, K. U., Prechtel, A., & Ray, N. (2018). Discrete-continuum multiphase model for structure formation in soils including electrostatic effects. *Frontiers in Environmental Science*, *6*, 96. https://doi.org/10.3389/fenvs.2018.00096

Schjønning, P., Thomsen, I. K., Møberg, J. P., de Jonge, H., Kristensen, K., & Christensen, B. T. (1999). Turnover of organic matter in differently textured soils: I. Physical characteristics of structurally disturbed and intact soils. *Geoderma*, *89*, 177–198. https://doi.org/10.1016/S0016-7061(98)00083-4

Schlüter, S., Leuther, F., Albrecht, L., Hoeschen, C., Kilian, R., Surey, R., Mikutta, R., Kaiser, K., Mueller, C. W., & Vogel, H.-J. (2022). Microscale carbon distribution around pores and particulate organic matter varies with soil moisture regime. *Nature Communications*, *13*, 2098. https://doi.org/10.1038/s41467-022-29605-w

Schweizer, S. A., Bucka, F. B., Graf-Rosenfellner, M., & Kögel-Knabner, I. (2019). Soil microaggregate size composition and organic matter distribution as affected by clay content. *Geoderma*, *355*, 113901. https://doi.org/10.1016/j.geoderma.2019.113901

Schweizer, S. A., Hoeschen, C., Schlüter, S., Kögel-Knabner, I., & Mueller, C. W. (2018). Rapid soil structure formation after glacial retreat driven by organic matter accrual at the microscale. *Global Change Biology*, *24*, 1637–1650. https://doi.org/10.1111/gcb.14014

Schweizer, S. A., Mueller, C. W., Höschen, C., Ivanov, P., & Kögel-Knabner, I. (2021). The role of clay content and mineral surface area for soil organic carbon storage in an arable toposequence. *Biogeochemistry*, *156*, 401–420. https://doi.org/10.1007/s10533-021-00850-3

Six, J., Elliott, E. T., & Paustian, K. (2000). Soil macroaggregate turnover and microaggregate formation: A mechanism for C sequestration under no-tillage agriculture. *Soil Biology and Biochemistry*, *32*, 2099–2103.

Soong, J. L., Phillips, C. L., Ledna, C., Koven, C. D., & Torn, M. S. (2020). CMIP5 models predict rapid and deep soil warming over the 21st century. *Journal of Geophysical Research: Biogeosciences*, *125*, e2019JG005266. https://doi.org/10.1029/2019JG005266

Souza, I., Almeida, L. F., Jesus, L. G., Kleber, M., & Silva, I. R. (2017). The mechanisms of organic carbon protection and dynamics of C-saturation in oxisols vary with particle-size distribution. *European Journal of Soil Science*, *68*, 726–739. https://doi.org/10.1111/ejss.12463

Stewart, C. E., Plante, A. F., Paustian, K., Conant, R. T., & Six, J. (2008). Soil carbon saturation: Linking concept and measurable carbon pools. *Soil Science Society of America Journal*, *72*, 379–392.

Swift, M. J., Heal, O. W., & Anderson, J. M. (1979). *Decomposition in terrestrial ecosystems*, *studies in ecology*. Blackwell, Oxford.

Totsche, K. U., Amelung, W., Gerzabek, M. H., Guggenberger, G., Klumpp, E., Knief, C., Lehndorff, E., Mikutta, R., Peth, S., Prechtel, A., Ray, N., & Kögel-Knabner, I. (2018). Microaggregates in soils. *Journal of Plant Nutrition and Soil Science*, *181*, 104–136.

Virto, I., Moni, C., Swanston, C., & Chenu, C. (2010). Turnover of intra- and extra-aggregate organic matter at the silt-size scale. *Geoderma*, *156*, 1–10. https://doi.org/10.1016/j.geoderma.2009.12.028

Vogel, C., Mueller, C. W., Hoschen, C., Buegger, F., Heister, K., Schulz, S., Schloter, M., & Kogel-Knabner, I. (2014). Submicron structures provide preferential spots for carbon and nitrogen sequestration in soils. *Nature Communications*, *5*, 2947. https://doi.org/10.1038/ncomms3947

Watteau, F., Villemin, G., Bartoli, F., Schwartz, C., & Morel, J. L. (2012). 0–20 µm aggregate typology based on the nature of aggregative organic materials in a cultivated silty topsoil. *Soil Biology and Biochemistry*, *46*, 103–114. https://doi.org/10.1016/j.soilbio.2011.11.021

Wilhelm, R. C., Lynch, L., Webster, T. M., Schweizer, S., Inagaki, T. M., Tfaily, M. M., Kukkadapu, R., Hoeschen, C., Buckley, D. H., & Lehmann, J. (2022). Susceptibility of new soil organic carbon to mineralization during dry-wet cycling in soils from contrasting ends of a precipitation gradient. *Soil Biology and Biochemistry*, *169*, 108681. https://doi.org/10.1016/j.soilbio.2022.108681

Witzgall, K., Vidal, A., Schubert, D. I., Höschen, C., Schweizer, S. A., Buegger, F., Pouteau, V., Chenu, C., & Mueller, C. W. (2021). Particulate organic matter as a functional soil component for persistent soil organic carbon. *Nature Communications*, *12*, 4115. https://doi.org/10.1038/s41467-021-24192-8

Xu, X., Schaeffer, S., Sun, Z., Zhang, J., An, T., & Wang, J. (2020). Carbon stabilization in aggregate fractions responds to straw input levels under varied soil fertility levels. *Soil and Tillage Research*, *199*, 104593. https://doi.org/10.1016/j.still.2020.104593

Young, I. M., & Crawford, J. W. (2004). Interactions and self-organization in the soil-microbe complex. *Science*, *304*, 1634–1637. https://doi.org/10.1126/science.1097394

Zech, S., Dultz, S., Guggenberger, G., Prechtel, A., & Ray, N. (2020). Microaggregation of goethite and illite evaluated by mechanistic modeling. *Applied Clay Science*, *198*, 105845. https://doi.org/10.1016/j.clay.2020.105845

Zech, S., Ritschel, T., Ray, N., Totsche, K. U., & Prechtel, A. (2022). How water connectivity and substrate supply shape the turnover of organic matter – Insights from simulations at the scale of microaggregates. *Geoderma*, *405*, 115394. https://doi.org/10.1016/j.geoderma.2021.115394

Zech, S., Schweizer, S.A., Bucka, F.B., Ray, N., Kögel-Knabner, I., & Prechtel, A. (2022). Data from: Explicit spatial modeling at the pore scale unravels the interplay of soil organic carbon storage and structure dynamics. Figshare [Dataset]. https://doi.org/10.6084/m9.figshare.19663986

SUPPORTING INFORMATION

Additional supporting information may be found in the online version of the article at the publisher's website.

How to cite this article: Zech, S., Schweizer, S. A., Bucka, F. B., Ray, N., Kögel-Knabner, I., & Prechtel, A. (2022). Explicit spatial modeling at the pore scale unravels the interplay of soil organic carbon storage and structure dynamics. *Global Change Biology*, *28*, 4589–4604. https://doi.org/10.1111/gcb.16230